Original article

Identification of potential inhibitors of Zika virus NS5 RNA-dependent RNA polymerase through virtual screening and molecular dynamic simulations

Noreen [a,b,*], Roshan Ali [a], Syed Lal Badshah [b], Muhammad Faheem [c], Sumra Wajid Abbasi [c], Riaz Ullah [d], Ahmed Bari [e], Syed Babar Jamal [c], Hafiz Majid Mahmood [f], Adnan Haider [c], Sajjad Haider [g]

[a] Institute of Basic Medical Sciences, Khyber Medical University, Peshawar, Pakistan
[b] Department of Chemistry, Islamia College University, Peshawar, Pakistan
[c] Department of Biological Sciences, National University of Medical Sciences, Rawalpindi, Pakistan
[d] Department of Pharmacognosy (MAPPRC), College of Pharmacy, King Saud University, Riyadh, Saudi Arabia
[e] Department of Pharmacuitcal Chemistry, College of Pharmacy, King Saud University, Riyadh, Saudi Arabia
[f] Department of Pharmacology, College of Pharmacy, King Saud University, Riyadh, Saudi Arabia
[g] Department of Chemical Engineering, College of Engineering, King Saud University, Riyadh, Saudi Arabia

ARTICLE INFO

ABSTRACT

Zika virus (ZIKV) is one of the mosquito borne flavivirus with several outbreaks in past few years in tropical and subtropical regions. The non-structural proteins of *flaviviruses* are suitable active targets for inhibitory drugs due to their role in pathogenicity. In ZIKV, the non-structural protein 5 (NS5) RNA-Dependent RNA polymerase replicates its genome. Here we have performed virtual screening to identify suitable ligands that can potentially halt the ZIKV NS5 RNA dependent RNA polymerase (RdRp). During this process, we searched and screened a library of ligands against ZIKV NS5 RdRp. The selected ligands with significant binding energy and ligand-receptor interactions were further processed. Among the selected docked conformations, top five was further optimized at atomic level using molecular dynamic simulations followed by binding free energy calculations. The interactions of ligands with the target structure of ZIKV RdRp revealed that they form strong bonds within the active sites of the receptor molecule. The efficacy of these drugs against ZIKV can be further analyzed through *in-vitro* and *in-vivo* studies.
© 2020 The Author(s). Published by Elsevier B.V. on behalf of King Saud University. This is an open access article under the CC BY-NC-ND license (http://creativecommons.org/licenses/by-nc-nd/4.0/).

1. Introduction

Zika virus (ZIKV) is one of the potential pandemic causing flavivirus in tropical and sub-tropical regions of the world. The Zika virus was first discovered in Africa during 1947 and was initially reported among Asians countries in 1966 (Musso et al., 2019). Zika virus is an arbovirus (arthropod-borne virus) categorized into the *flavivirus* genus within the family of *flaviviridae* (Saiz et al., 2016). Flaviviruses are small enveloped single stranded positive RNA

viruses (Kazmi et al., 2020). Zika virus is about 11 kb positive-sense RNA virus (Chan et al., 2016; Chen and Hamer, 2016). The genome encodes 3419 amino acids along with two flanking untranslated regions (3′ and 5′ untranslated regions) and a single long open reading frame encoding a polyprotein that is folded in capsid (C), precursor of membrane (prM), envelope (E) and 7 non-structural (NS) proteins (50-C-prM-ENS1-NS2A-NS2B-NS3-NS4A-NS4B-NS5-30). The single long open reading frame provides the shape to secondary structures, which are essential for translation and replication of virus's genome. RNA-dependent RNA polymerase NS5 of Zika weighs about 103 kDa (Ramharack and Soliman, 2018; Upadhyay et al., 2017; Wang et al., 2017, 2018; Zhao et al., 2017). It performs the capping of genomes in the cytoplasm and replicates the viral positive and negative RNA genome. It causes methylation of viral RNA cap at guanine N-7 and ribose 2′-O positions. It also prevents the establishment of cellular antiviral state by blocking the IFN-alpha/beta signaling pathway besides its role in RNA genome replication. It prevents activation of

* Corresponding author at: Department of Chemistry, Islamia College University, Peshawar, Pakistan. Tel.: +92-346-971-3604.
E-mail address: Noreenkhattak777@gmail.com (Noreen).

JAK-STAT signaling pathway by inhibiting host TYK2 and STAT2 phosphorylation. It has been extensively used as a site to intervene antiviral drugs due to its vital role (Best, 2017; Chaudhary et al., 2017).

Computational drug designing has lowered the cost of novel drug research and is saving time and resources (Ahmad et al., 2020a; Zhang, 2011). The obtained results are analyzed through several ways (Ou-Yang et al., 2012). It is therefore important to resolved the various enzymatic structure using X-ray crystallography and NMR methods to better understand the re-emerging Zika virus (Lionta et al., 2014). The World Health Organization (WHO) declared Zika virus as a public health emergency in February 2016 and several studies linked the virus with fetal microcephaly (Badshah et al., 2018) and various other neural defects has been proved. There are several high resolution structures available for the envelope protein along with all soluble and non-structural proteins of the Zika virus (Badshah et al., 2017; Hilgenfeld, 2016). Structure-based antivirals agents against ZIKV can be designed, as there are several crystallographic structures available in the protein data bank. Various identified inhibitors showed that they stop ZIKV replication. Different methods comprising repurposing the

medications previously used in practice for various infections and screening of different compounds libraries using computational approach is beneficial. The 3D structure based drug designing is more effective than the discovery of a drug by traditional ways (Ahmad et al., 2017). This method utilized the details of 3D arrangement of a target in the ongoing procedure and also aims to know the molecular basis of disease (Lionta et al., 2014). The computational study reduces the time; cost, chances of error and help in selection of best possible drugs through this method. The Zika virus's NS5 polymerase is the most active target for inhibition due to its significant part in virus replication (Ahmad et al., 2020b; Parkinson and Pryde, 2010). In case of Zika virus, few lead compounds i.e. 3-chloro-N-[({4-[4-(2-thienylcarbonyl)-1-piperazinyl] phenyl}amino) carbonothioyl]-1-benzothiophene-2-carboxamide (TPB) (Pattnaik et al., 2018), Andrographolide (code: ZINC03881797) (Feranchuk et al., 2016) and ZINC39563464 (Ramharack and Soliman, 2018) are identified against the 3D structure of ZIKV polymerase by virtual screening approach. In these studies, the 3D models of ZIKV RdRp enzyme were homology modelled using the structures of other *flaviviral* polymerases as a template. These compounds interacted inside the receptor cavity with very few binding residues. These studies open a window for further investigations for designing inhibitory molecules against the ZIKV RdRp (Godoy et al., 2017; Pattnaik et al., 2018). The crystallographic structures of ZIKV RdRp showed more functional binding cavities as compare to the previously modeled structures based on other *flaviviruses*. There are only few lead compound identified for the crystal structure of ZIKV polymerase that showed good binding interactions (Feranchuk et al., 2016; Pattnaik et al., 2018; Ramharack and Soliman, 2018). Therefore, identification of more such inhibitors against the 3D structure of Zika polymerase is highly sought (Ahmad et al., 2020b). The aim was to find out potent inhibitors against the ZIKV NS5 RdRp polymerase by computational method. Here in this study, through virtual screening, we identify drug candidate molecules in vast library of compounds that can potentially inhibit the Zika virus' NS5 RNA-dependent RNA polymerase.

2. Material and methods

2.1. Target structure preparation

The crystal structures of NS5 RNA-Dependent RNA Polymerase of ZIKV were obtained from the RCSB Protein Data Bank (PDB) (Burley et al., 2017; Gore et al., 2017; Goodsell et al., 2020) under the accession codes 5u0c (Zhao et al., 2017a), 5u04 (Godoy et al., 2017), 5wz3 (Duan et al., 2017b), 5u0b (Zhao et al., 2017a) and 5ftr (Upadhyay et al., 2017). Discovery studio visualizer (Studio, 2009) was used for the analysis of all 3D structures of target enzyme. The 5ftr consists of two identical chains A and B with 267–887 residues while 5u0b is also composed of two similar A and B chains with 265–887 residues. The 5u0c consists of eight parallel chains A, B, C, D, E, F, G, H with 268–891 residues while 5u04, and 5wz3 are present with one chain A with 321–887 and 274–887 residues respectively. Before superimposition of ZIKV polymerase 3D structures, it was necessary to arrange all the structures. The 5wz3 and 5u04 are present with some missing residues at specific regions i.e. 313–321, 342–347, 406–425, 455–476 and 340–364, 408–417, 454–471, 533–542, 576–606, 689–695 respectively. Although these structures have high resolution i.e. 1.8A° for 5wz3 and 1.9A° for 5u04but then 5u04 was excluded from the study due to high number of missing residues as compare to 5wz3. Repeated chains were removed from the remaining three structures i.e. 5ftr, 5u0b and 5u0c and they were arranged in terms of chain length similar to 5wz3 i.e. 274–887. Now all structures
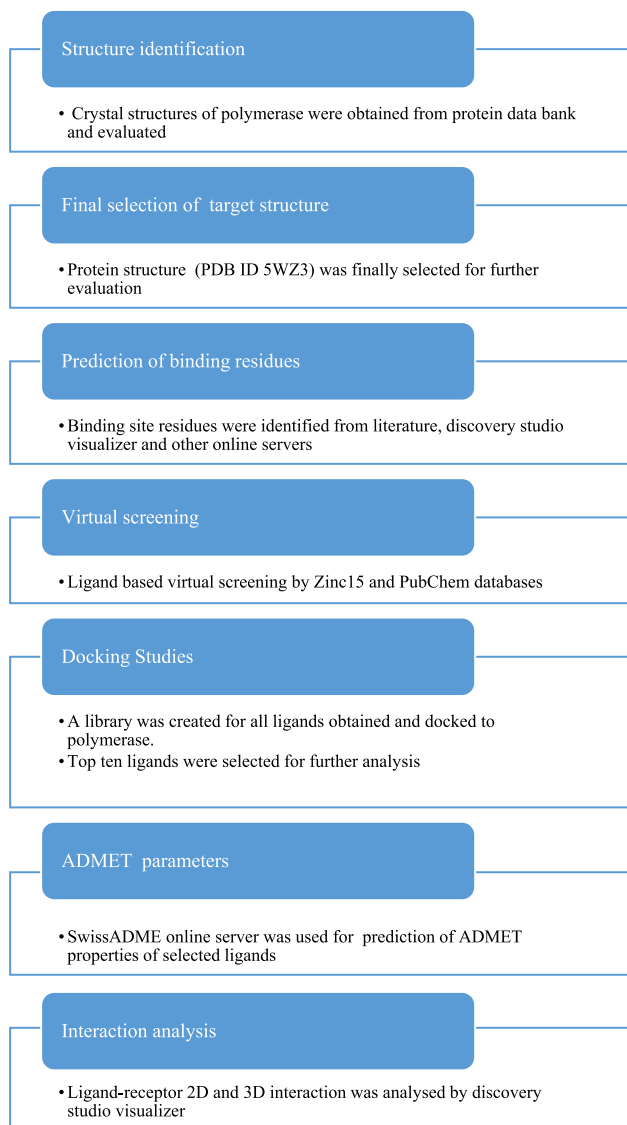
Fig. 1. Flow chart showing virtual screening process for Zika virus polymerase (PDB ID 5WZ3).
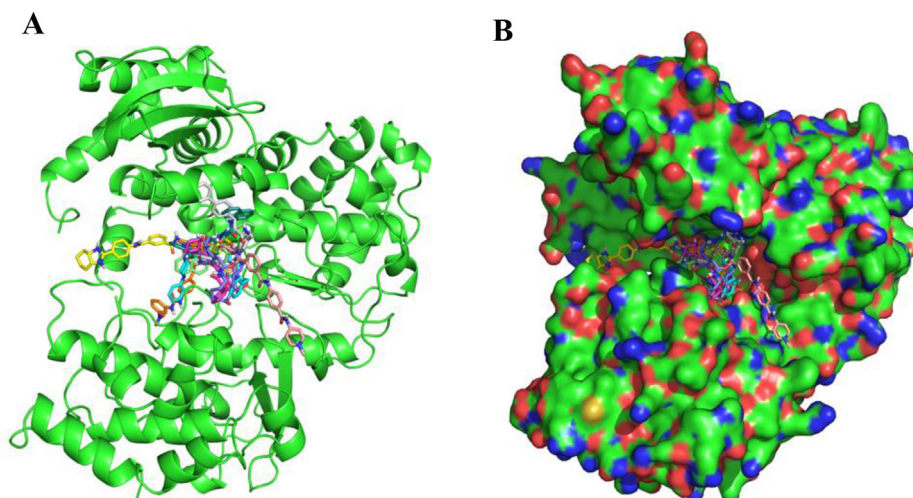
Fig. 2. Protein structure of Zika virus NS5 protein (PDB ID 5WZ3) in complex with docked compounds (sticks) at the active site pocket as shown in (A) Cartoon presentation and (B) Surface view.

were almost present with similar number of residues i.e. 274–887. Structures except 5wz3 (due to missing residues) were superimposed by discovery studio visualizer (Studio, 2009). Alignment of sequences was also done by discovery studio visualizer (Studio, 2009). The 5u0b and 5u0c have 3A^O resolution while 5ftr has 3.05A^O resolution. We also dropped 5ftr from the study due to low resolution as compared to 5u0b and 5u0c. Theroot mean square deviation (RMSD) values of the rest of two structures were 0.27 for the 5u0c and 0.36 for the 5u0b. We processed the 5u0b ZIKV crystal structure as possible target for virtual screening due to the RMSD value.5wz3 was also included in study due to its high resolution i.e. 1.8A^o. Finally, two target structures, 5wz3 and 5u0b with high resolution were further processed. The sequences of 5wz3 and 5u0b were further aligned by CLC Sequence Viewer 8 (Bio-Qiagen, 2016).

2.2. Identification of binding site

The binding residues of 5wz3 and 5u0b were identified from literature (Duan et al., 2017; Zhao et al., 2017a), discovery studio visualizer (Studio, 2009) and online servers i.e. Findsite (Brylinski and Skolnick, 2008), Coach (Yang et al., 2013), Tm–Site (Yang et al., 2013), S-site (Yang et al., 2013), Cofactor (Zhang et al., 2017), Concavity (Capra et al., 2009) and 3D LigandSite (Wass et al., 2010). Most of the residues were common among all the servers and in literature for both of the target structures. Among them, the most important and functional residues, mentioned in literature, were selected as target binding residues for virtual screening and docking study. According to the literature, both structures contain similar binding residues. Therefore, it was significant to select one target structure to simplify the whole process. On superimposition of the two structures, the common binding residues were clearly observed. The 5wz3 was selected as a final target for virtual screening.

2.3. Virtual screening and ligand–receptor interaction

Various reports are present about different ligands against the *flaviviruses* in published research studies. Five different molecules HeE12Tyr (PubChemID:122172828), Sofosbuvir (PubChemID:73425384), NITD008 (PubChemID:44633776), 7-Deaza-2′-C-methyl adenosine (7DMA) (PubChemID:3011893) (Wang et al., 2018) and TPB (Pattnaik et al., 2018) (PubChem ID: 1619825) are

reported to have inhibitory actions against *flaviviruses*. The three dimensional structures of these five inhibitory molecules were obtained from PubChem (Kishimoto et al., 2008) and Zinc15 databases (Irwin and Shoichet, 2005). Therefore, molecules having similarity to these five ligands might have potential to inhibit the Zika NS5 polymerase. For this purpose, we implemented the ligand based virtual screening using Zinc15 and PubChem databases. These two databases contained millions of purchasable "drug-like" compounds, effectively all organic molecules that are for sale, a quarter of which are available for immediate delivery. It connects purchasable compounds to high-value ones such as metabolites, drugs, natural products and annotated compounds from the literature. They offer new analysis tools that are easy for non-specialists yet with few limitations for experts. These databases retain their original 3D roots and all molecules are available in biologically relevant, ready-to-dock formats. Thus, these databases are useful source of ligand screening. The similarity index was at 70% for Zinc15, and 80% for PubChem. In Zinc15 and PubChem, we screened 537 and 405 similar structures respectively. Structure based virtual screening was carried out by pep:MMs:MIMIC (Floris et al., 2011) and MTiOpenScreen (Rey et al., 2015) online tools. A library was created for all ligands that were obtained from PyRx software (Dallakyan and Olson, 2015). PyRx uses AutoDock 4 and AutoDockVina as docking tools. We performed the docking into the binding site residues inside a grid box with X, Y and Z-axis and dimensions adjusted to 20.74 Å × 20.96 Å × 11.75 Å for the receptor molecule. The top ranked molecules were selected for further analysis. Discovery studio visualizer (Studio, 2009) was used to analyze the interaction between the docked ligands and the crystal structure of ZIKV RNA dependent RNA polymerase.

2.4. Analysis of pharmacokinetics

Molecular properties and drug likeness of top selected ligands were predicted by online web server i.e. SwissADME (Daina et al., 2017) (see Fig. 1).

2.5. Molecular dynamic simulations

The top five docked poses with lowest binding affinities were further subjected to molecular dynamic (MD) simulations to gain a better insight into the interaction mechanism, using the same methodology as stated in our previous work (Abbasi et al., 2016).

All five simulations were conducted using AMBER 18 software (Song et al., 2019). The stability of complexes was tested by calculating the RMSDs of the resulting trajectories produced using AmberTools18′s CPPTRAJ module.

2.6. Binding free energy calculations

For all the five systems, binding free energy calculations were performed using the MMPBSA/GBSA methods to verify the docking results and to rescore the results (Miller III et al., 2012). Calculations have been made on snapshots taken from the MD trajectories using the same protocol previously reported by Abro and Azam (Abro and Azam, 2016).

3. Results and discussion

3.1. Target structure preparation

The superimposed 3D structures of ZIKV polymerase, multiple and pairwise sequence alignment of selected structures is shown in supplementary data.

3.2. Identification of binding site

Literature shows alanine 409, leucine 410, glycine 411, glutamate 439, histidine 443, cysteine 448, 451, arginine 473, glycine 538, lysine 691, histidine 714, asparagine 716, cysteine 730, 849, aspartate 665, 666, 535, arginine 363, glutamine 598, asparagine 576 and tryptophan 797 (Zhao et al., 2017a) as binding pocket for 5u0b and glutamate 439, histidine 443, cysteine 448, 451, histidine 714, cysteine 730, 849, aspartate 665, aspartate 666, aspartate 535, arginine 363, glutamine 598, arginine 576 and tryptophan 797 (Duan et al., 2017) for 5wz3. Discovery studio visualizer (Studio, 2009) predicted alanine 409, leucine 410, glycine 411, glutamate 439, histidine 443, cysteine 448, 451, arginine 473, glycine 538, lysine 691, histidine 714, asparagine 716, cysteine 730, 849 for 5u0b and glutamate 439, histidine 443, cysteine 448, 451, histidine 714, cysteine 730, 849 for 5wz3. The binding pockets predicted by other online servers are shown in table in supplementary data.

3.3. Selection of binding pocket and target structure

Glutamate 439, histidine 443, cysteine 448, 451, histidine 714, cysteine 730, 849, aspartate 535, 665, 666, tryptophan 797, serine 798, histidine 800 and glycine 801 were selected as binding pocket for 5u0b and 5wz3 from literature study (Duan et al., 2017; Zhao et al., 2017a) and online servers' results. The most important and functional residues (Duan et al., 2017; Zhao et al., 2017a) including glutamate 439, histidine 443, cysteine 448, 451, histidine 714, cysteine 730, 849, aspartate 535, 665, 666, tryptophan 797 were selected as target binding site for docking studies. After superimposition, 5wz3 was finally selected as target structure due to its high resolution. Superimposed structures are shown in supplementary figures. In a previous study (Pattnaik et al., 2018), one lead compound, TPB was identified to stop the ZIKV polymerase activity against the 3D model of Zika polymerase that was created by homology modeling using the RNA-dependent RNA polymerase of DENV-3 as the crystal structure of ZIKV polymerase wasn't solved till that time. The compound also showed its inhibitory activity *in vivo* and *in vitro* analysis. TPB was docked against a cavity with very few binding residues i.e. Aspartate 535, 665 and 666 which are required for action of polymerase enzyme. In order to initiate the ribonucleotide polymerization, these residues have important roles. They coordinate with two metal ions (Mg^{2+})

(Butcher et al., 2001; Choi and Rossmann, 2009; Duan et al., 2017; Ng et al., 2008; Yap et al., 2007). The study presented a perspective for further investigations for anti ZIKV inhibitory molecules against the recently solved crystal structure of ZIKV polymerase (Godoy et al., 2017; Pattnaik et al., 2018). The structure identified more functional binding residues as compare to the 3D model of ZIKV polymerase based on Dengue polymerase structure as discussed in previous study (Pattnaik et al., 2018) i.e. glutamate 439, histidine 443, cysteine 451, histidine 714, cysteine 730 and 849, aspartate 665, 666 and 535, and tryptophan 797. Glutamate 439, histidine 443 and cysteine 451 constitute the finger domain. They are the main coordinating amino acids of zinc binding site. Histidine 714, cysteine 730 and 849 constitute the thumb domain and they are the main coordinating amino acids of zinc binding site. Tryptophan 797 assembles with the first nucleotide and initiates the *de novo* synthesis of RNA. Thus the recently solved crystal structure provides more binding residues as compare to the 3D model of ZIKV polymerase based on Dengue polymerase structure as discussed in previous study (Pattnaik et al., 2018). In one study (Feranchuk et al., 2016), the lead compound ZINC03881797 (Andrographolide) was selected as best candidate for ZIKV polymerase where only one binding residue (Glutamate 547) was taken as target site for docking studies. In another study, ZINC39563464 (Ramharack and Soliman, 2018) was identified as potent inhibitor during virtual screening where few residues were selected for binding of ligand.

3.4. Virtual screening

The development of small nucleoside inhibitors in recent years, aims to block the functional activities of polymerases of *flaviviruses*. It has been an encouraging treatment strategy towards *flaviviral* diseases (Boldescu et al., 2017; Malet et al., 2008). For instance, the Federal Drug Administration (FDA) of USA approved the HCV NS5B polymerase nucleoside inhibitor named sofosbuvir to treat the infection of HCV. Furthermore, the *in vitro* studies recently demonstrated that sofosbuvir antagonized ZIKV genome replication in human cells. This showed that sofosbuvir is a possible potential drug candidate against ZIKV infection showing its broad anti-*flaviviridae* activity. These *in vitro* cellular assays could assist in the screening of potent inhibitors based on anti-*flaviviral* sofosbuvir, against the ZIKV RdRp, and further validation of novel inhibitors of ZIKV replication. In this framework, computational methods would be able to knowingly contribute into both identifying molecular target structures and designing drug candidates with improved properties (Keating and Vaidya, 2014). In the current study, the ligand based virtual screening was carried out in which sofosbuvir was used as standard drug to screen the novel inhibitors by Zinc15 and PubChem databases. Total 233 and 100 molecules were screened by Zinc15 and PubChem databases respectively. The polymerase structures are highly resembled among *flaviviridae* members that encourage the efforts to re-use earlier identified anti-NS5 inhibitors for ZIKV NS5 polymerase. For example, the previously identified potent inhibitor for HCV, 7DMA exhibited high potential against ZIKV in cellular assays (Olsen et al., 2004). According to previous studies (Keating and Vaidya, 2014), these findings are helpful for screening of novel inhibitors by computational methods. Total 105 and 100 molecules were screened by Zinc15 and PubChem databases during virtual screening. Likewise, NITD008, another candidate molecule, was observed to have wide-ranging antiviral properties against ZIKV, HCV and all four serotypes of Dengue virus. It could be used to screen potential molecules by virtual screening (Wang et al., 2018). During the current study, total 44 and 100 molecules were identified by screening Zinc15 and PubChem databases respectively. Another drug, HeE1-2Tyr, also exhibits anti-*flaviviral* activity (Wang et al., 2018).

As discussed above, the *in vitro* cellular assays could allow the screening and validation of potent inhibitors based on anti- *flavivirals*, against the ZIKV RdRp. In the current study in Zinc15 and PubChem databases, we screened a total of 141 and 100 molecules. TPB (Pattnaik et al., 2018) showed its inhibitory activity against Zika polymerase during both *in silico* and *in vitro* analysis. In order to provide some more inhibitory molecules similar to TPB, ligand based virtual screening was performed. Zinc15 and PubChem databases screened total 14 and 5 molecules respectively. During current study, among the previously identified compounds by *in vitro* analysis, only one compound, HeE1-2Tyr has led to the identification of potent candidates i.e. ligand 56,949,972 and ligand ZINC000082155264 with high binding affinity against the ZIKV RdRp. Therefore, these results showed that these ligands could be further analyzed and validated by experimental studies against ZIKV RdRp. Table 1 shows the ligands that are obtained based on five standard ligands during virtual screening. Similarly, Table 2 shows the total ligands obtained based on 3D structure of Zika polymerase during virtual screening.

3.5. Molecular docking studies and pharmacokinetics

We performed the docking studies for ligands and receptor molecule through the PyRx software that uses AutoDock 4 and AutoDockVina as docking tools as discussed in earlier section. We tabulated the results with the binding Affinity (kcal/mol) values when calculations are complete. The docked ligand-receptor complexes were ranked based on binding affinity with lowest energy to be at the top. The top ten ranked ligand molecules are shown in the Table 3. All ligands were observed to follow the Lipinski's rule of five i.e. molecular weight less than 500 Da, hydrogen bond donor less than 5, hydrogen bond acceptors less than 10, log p-value not more than 5. The Table 3 also shows the chemical structures of these compounds. Selected molecules also shown appropriate ADMET properties. Their further implementation and optimization could be possible by *in vivo* assays and other experimental studies in order to validate the identified drug molecules against the targeted ZIKV RdRp. It will be useful for the researchers to discover effective inhibitory molecules against Zika viral targets. Thus, it can provide a wide range of antiviral agents in the future. The results of the computational study may vary if they are tested in laboratory environment but in most of the cases, it showed close proximity under proper conditions.

3.6. Ligand-receptor interactions

The interactions of top ten ligands with receptor molecule was analyzed in detail. The 3D representation of interactions of top ligands with target structure is shown in supplementary figures. Fig. 2 shows the cartoon presentation and surface view while Fig. 3 shows the 2D representation of interactions. Hydrogen bonds play various roles cellular processes. They promote molecular interactions such as protein–ligand interactions (Chen et al., 2016). All suggested lead molecules interact through hydrogen bonds with catalytic residues of NS5 RdRp. In previous study (Pattnaik et al., 2018), the TPB compound formed three hydrogen bonds with aspartate 535 and aspartate 665. While in the current study, the ligand MMs02998601 was observed to interact with active site residues of polymerase by forming six hydrogen bonds with threonine 795, threonine 796, glycine 801, glutamine 605, valine 606 and glycine 604 (Fig. 3, A). Current study suggests that ligand MMs02998601 with more molecular interactions with the highly resolved 3D structure of Zika NS5 polymerase may show more inhibitory activity as compare to TPB compound. In the same manner ligand 2 formed hydrogen bond with serine 603, aspartate 540 (Fig. 3, B), ligand 3 formed no hydrogen bond with the receptor

(Fig. 3, C). Ligand 4 was observed to form hydrogen bond with arginine 731 (Fig. 3, D), ligand 5 with aspartate 665 (Fig. 3, E), ligand 6 with aspartate 665, asparagine 612, glycine 664 (Fig. 3, F). The ligand 7 formed hydrogen bond with serine 798, serine 663, serine 712, glycine 664, glutamine 605 (Fig. 3, G), ligand 8 with isoleucine 799, serine 798, histidine 800 (Fig. 3, H), and ligand 9 with tyrosine 609, aspartate 665, aspartate 666, serine 712, histidine 714 (Fig. 3, I). The ligand 10 interacted through hydrogen bonding with the NS5 RdRp with serine 663, aspartate 540 (Fig. 3, J), and ligand 11 with valine 606, glutamine 605, arginine 483, glutamine 605, asparagine 494, ligand 12 with glycine 604 of the ZIKV RdRp. The ligand 13 formed interactions with valine 606, ligand 14 with isoleucine 799, tyrosine 609, tryptophan 797, serine 798, serine 663, glutamine 605 of ZIKV NS5 RdRp. The ligand 15 formed no hydrogen bond with the target structure, ligand 16 interacted with arginine 483, valine 606, asparagine 494, ligand 17 with glutamine 605, arginine 483 of ZIKV NS5 RdRp. The ligand 18 also formed no hydrogen bonding, while ligand 19 interacted with the ZIKV NS5 RdRp through asparagine 494 and ligand 20 formed hydrogen bond with arginine 794 and 483. The *in-vitro* and *in-vivo* analysis of top ten ligands will further help in exploring their true potency against ZIKV. The interaction of these ligands with the ZIKV polymerase suggests that further analysis of these inhibitory molecules may provide a path towards the effective treatment of ZIKV in future.

3.7. Molecular dynamic simulations

Molecular dynamics simulation is an important computational technique for exploring the stable behavior of protein ligand docked complexes under various physiological conditions. During the simulation of 20 ns, for each docked complex, RMSD plots were created using the backbone coordinates of docked complexes to determine the possible structural deviations and to assess the stability of complexes (Fig. 4). It was observed that stability was achieved after 2 ns for all the docked complexes, except ZIKV RdRp-MMs02321984 complex. For the ZIKV RdRp-MMs02321984 stability was attained after 4 ns. Fig. 4 indicates that the highest average RMSD value was observed for MMs02321984, while MMs02998601 had the lowest average RMSD value. MMs02998601 reached equbillirium around 1.8 ns and remain stable till the end of simulation run with an average RMSD of 1.69 Å. MMs02899945 attained the equibilirum after 0.8 ns, but about 7 ns small fluctuation with a gradual increase in RMSD from 2.1 Å to 2.7 Å were seen. Afterwards, the system remained stable at an average RMSD value of 2.07 Å. MMs02517431 also showed more or less simliar trend like MMs02899945 with an average RMSD of 1.85 Å. ZIKV RdRp- MMs02374310 complex reached an equilibrium after 1.6 ns and subsequently showed the stable beha-

Table 1
Table showing the total ligands obtained during ligand based virtual screening via Zinc15 and PubChem databases.

S. No	Database	Ligands
1	Zinc15	537
2	PubChem	405

Table 2
Table showing the total ligands obtained during structure based virtual screening via MTIOpenscreen and Pep:MMs:MIMIC databases.

S. No	Database	Ligands
1	MTIOpenscreen	100
2	Pep:MMs:MIMIC	200

Table 3

Table showing the ligands selected during virtual screening, their library codes, chemical names, structures, and their protein interaction residues along with binding energies.

S. No	Library code	IUPAC name	Chemical structure	Interacting residues	Binding energy
01.	MMs02998601	1-(3-nitrophenyl)-3-[4-[4-[(3-nitrophenyl) carbamoylamino] benzyl] phenyl]urea		Gly604, Gln605, Val606, Arg794, Thr795, Thr796, Ile799, Gly801	−10.1
02.	MMs02899945	(E)-3-phenylacrylic-acid-[4-[(E)-[[2-keto-2-(1-naphthylamino) acetyl] hydrazono] methyl] phenyl]-ester		Lys359, Trp476, Asp540, Ser603, Trp797	−10
03.	MMs02321984	N,N'-bis[4-[(3aR,7aS)-3a,4,5,6,7,7a-hexahydro-1H-benzimidazol-3-ium-2-yl] phenyl] isophthalamide		Lys403, Val404, Arg483, Val606	−9.9
04.	MMs02517431	2-(oxoBLAHylidene)-N-[4-[2-(oxoBLAHylidene) acetyl] aminobutyl] acetamide		Arg731	−9.8
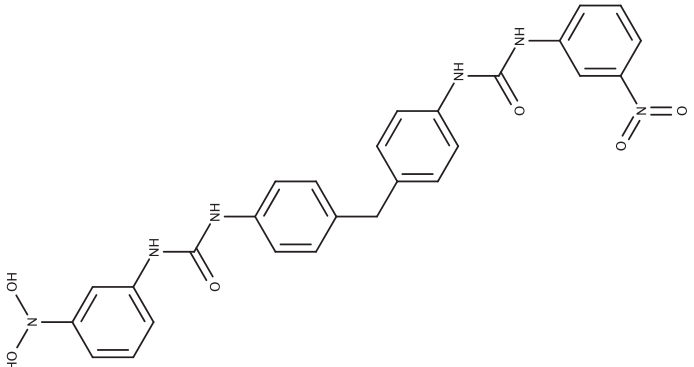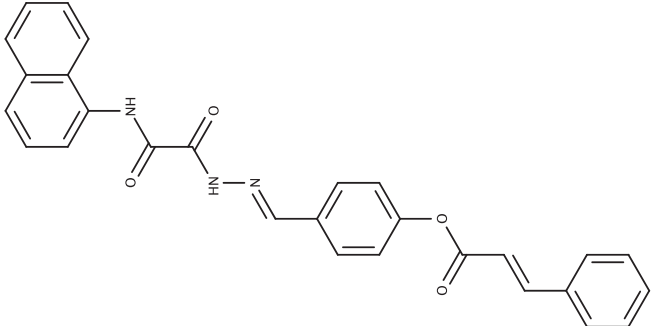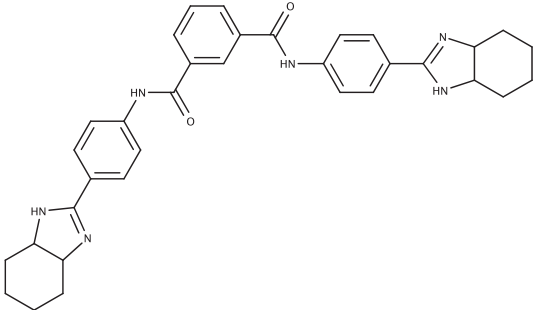
Table 3 (continued)

S. No	Library code	IUPAC name	Chemical structure	Interacting residues	Binding energy
05.	MMs02374310	N-[2-(1H-indol-3-yl) ethyl]-4-[[[(E)-3-(4-phenylphenyl) acryloyl] amino] methyl] benzamide		Val355, Met455,Trp476, Asp665, Trp797	−9.5
06.	MMs03915724	[4-[2-(1-naphthyloxy) propanoylaminoiminomethyl] phenyl]		Asp540, Asn612, Gly664, Asp665, Ile799	−9.3
07.	MMs00951683	N-[3-[4-(2-fluorophenyl) piperazin-1-yl] propyl]-2,4-dioxo-3-phenethyl-1H-quinazoline-7-carboxamide		Gln605, Tyr609, Ser663, Gly664, Cys711, Ser712, Ser798, Ile799	−9.3
08.	56,949,972	8-(cyclohexoxy)-1,5,5-trioxo-2-phenyl-pyrido[2,1-b]		Arg731, Trp797, Ser798, Ile799,	−9
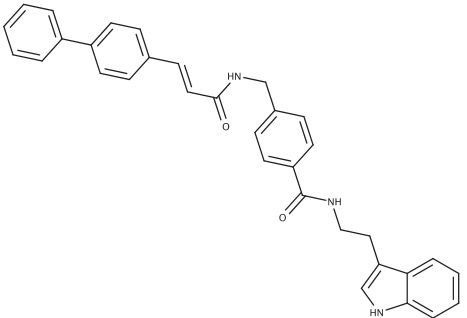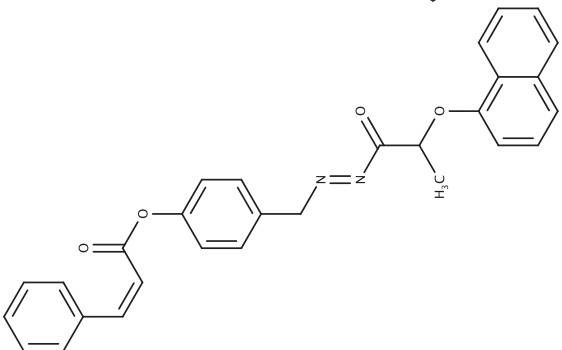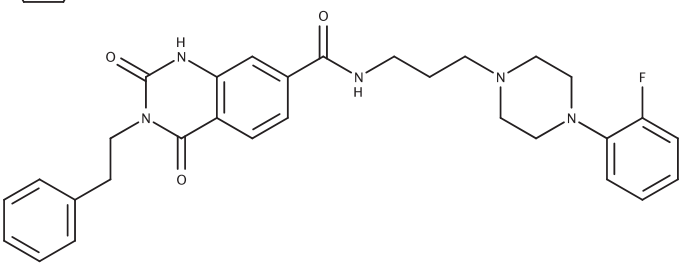
Table 3 (*continued*)

S. No	Library code	IUPAC name	Chemical structure	Interacting residues	Binding energy
	(PubChem)	[1,3] benzothiazole-4-carboxylic acid		His800	
09.	MMs02329489	N,N'-bis[4-[(1-methylpyridin-1-ium-4-yl)carbamoyl] phenyl] isophthalamide		Tyr609, Asp665, Asp666, Pro709, Ser712, His714	−9
10.	ZINC000082155264	8-(cyclohexoxy)-1-oxo-2-phenyl-pyrido[2,1-b][1,3] benzothiazole-4-carboxylic		Asp540, Tyr609, Ser663, Asp665	−8.9
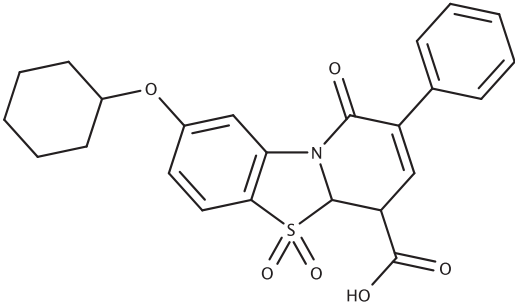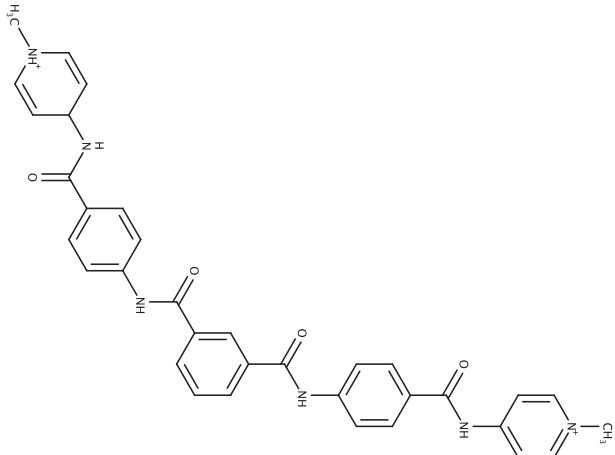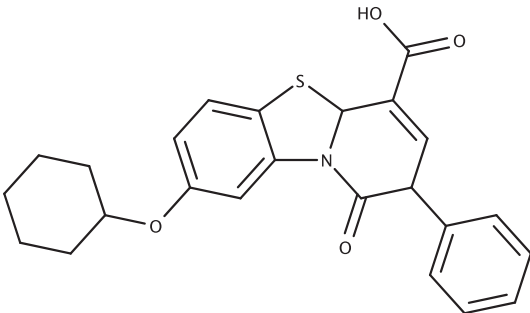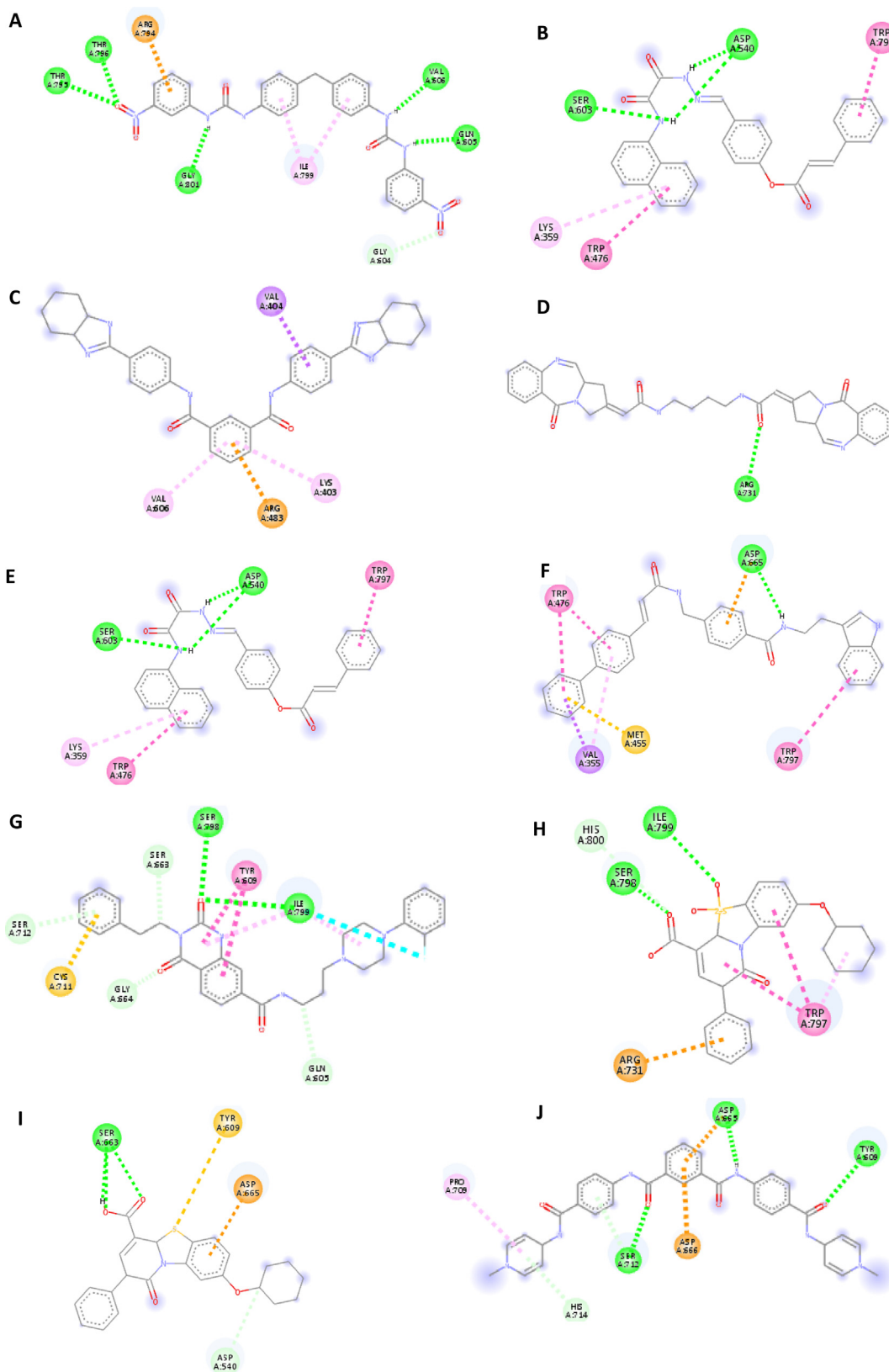
Fig. 3. (A) 2D representation of interaction between MMs02998601 and target residues of ZIKV NS5 polymerase. (B) 2D representation of interaction between MMs02899945 and target residues of ZIKV NS5 polymerase. (C) 2D representation of interaction between MMs02321984 and target residues of ZIKV NS5 polymerase. (D) 2D representation of interaction between MMs02517431 and target residues of ZIKV NS5 polymerase. (E) 2D representation of interaction between MMs02374310 and target residues of ZIKV NS5 polymerase. (F) 2D representation of interaction between MMs03915724 and target residues of ZIKV NS5 polymerase. (G) 2D representation of interaction between MMs00951683 and target residues of ZIKV NS5 polymerase. (H) 2D representation of interaction between 56949972 (PubChem) and target residues of ZIKV NS5 polymerase. (I) 2D representation of interaction between MMs02329489 and target residues of ZIKV NS5 polymerase. (J) 2D representation of interaction between ZINC000082155264 and target residues of Zika NS5 Polymerase.
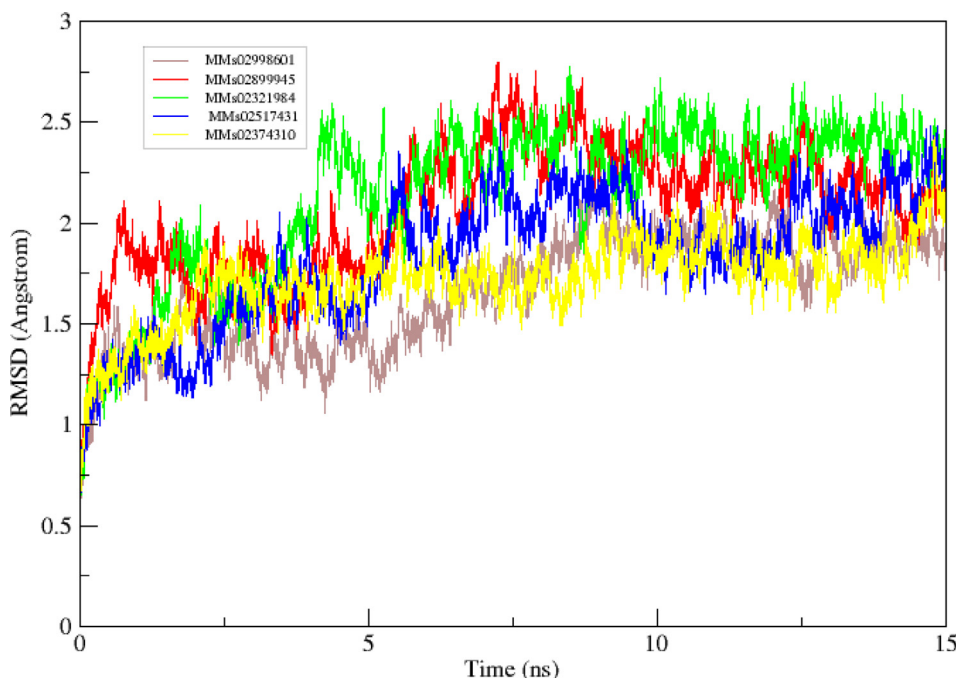
Fig. 4. RMSDs of backbone atoms (C, Cα, N) for protein of each docked complex with respect to time. Color key: brown **MMs02998601**, red **MMs02899945**, green **MMs02321984,** blue **MMs02517431** and yellow **MMs02374310.**

viour afterwards with an average RMSD of 1.73 Å. Overall, the findings of RMSD support the conformational stability of selected systems and supports the docking results.

3.8. Binding free energy calculations

The top five ligands were rescored on the basis of free energies calculated using MMPBSA/GBSA methods. All the energy values were calculated as the average value of 100 snapshots from the entire MD trajectories. In the case of MMGBSA, the total free energies (ΔG_{TOT}) calculated for the docked complexes were between -39.5403 kcalmol^{-1} and -16.0912 kcalmol^{-1}, while for MMPBSA method, the values were between -34.8923 kcalmol^{-1} and -19.9685 kcalmol^{-1}, shown in Table 4. Among the five complexes analyzed, MMs02321984 had the high energy values (-39.5403 and -34.8923 kcalmol^{-1}), followed by MMs02998601 (-39.2669 and -29.7642 kcalmol^{-1}) whereas MMs02517431 had the lowest (-16.0912 and -19.9685 kcalmol^{-1}). It was noted that the van der Waals interactions, total energy of solute (ΔG_{GAS}) and non-polar contribution (ΔE_{NPOL}), all of which were negative,

contributed favorably to binding affinities. The net energy values calculated have shown that the MMs02321984 complex, ranked 3rd in docking, is more stable than the MMs02998601 complex, ranked 1st on the basis of docking socre. Based on total ΔG_{TOT} MMs02321984 ranked 1st, MMs02998601 ranked 2nd, MMs02374310 ranked 3rd, MMs02899945 ranked 4th and MMs02517431 ranked 5th. However, the energy values estimated for top five docked hits are still within the appropriate range and confirm the stabililty of docked complexes. Overall, the findings of MD simualtion and MMPBSA/GBSA are consistent with the docking results and it is expected that these reuslts would be helpful in future designing of potent ZIKV RdRp inhibitors.

4. Conclusion

To reduce the cost of drug development and to limit the extent of time, virtual screening methods and docking studies for drug discovery are used widely. Few lead compounds are available that inhibit the ZIKV NS5 RNA dependent RNA polymerase. The current study provides new insights about different novel ligands as inhi-

Table 4
Binding free energies value calculated using MMGBSA and MMPBSA for the top five complexes.

Method	Energies	MMs02998601	MMs02899945	MMs02321984	MMs02517431	MMs02374310
MMGBSA	ΔE_{VDW}	−57.7514	−40.0304	−59.5976	−50.6025	−46.1716
	ΔE_{EEL}	−18.0576	0.8603	−14.1306	−39.6230	−25.0981
	ΔE_{GB}	43.2317	14.7780	40.7199	79.1666	49.7507
	ΔE_{SURF}	−6.6896	−3.5401	−6.5320	−5.0322	−5.9868
	ΔG_{gas}	−75.8090	−39.1701	−73.7282	−90.2256	−71.2697
	ΔG_{solv}	36.5421	11.2380	34.1879	74.1344	43.7638
	ΔG_{TOT}	−39.2669	−27.9321	−39.5403	−16.0912	−27.5058
MMPBSA	ΔE_{VDW}	−57.7514	−40.0304	−59.5976	−50.6025	−46.1716
	ΔE_{EEL}	−18.0576	0.8603	−14.1306	−39.6230	−25.0981
	ΔE_{PB}	51.9488	16.5149	44.5310	73.9166	49.4116
	ΔE_{NPOL}	−5.9040	−2.9186	−5.6951	−3.6595	−5.4709
	ΔE_{DISPER}	0.0000	0.0000	0.0000	0.0000	0.0000
	ΔG_{gas}	−75.8090	−39.1701	−73.7282	−90.2256	−71.2697
	ΔG_{solv}	46.0448	13.5962	38.8359	70.2571	43.9408
	ΔG_{TOT}	−29.7642	−25.5738	−34.8923	−19.9685	−27.3289

bitors for the crystal structures of ZIKV NS5 RNA dependent RNA polymerase using virtual screening. Here we presented appropriate binding pockets for ligand molecules. We choose the top ten ligands based on their binding affinities with the target structure. Lastly, to optimize and validate the docking results, the top five complexes having good binding affinity and accurate docking poses were further refined and rescored through the MD simulations, and MMPBSA/GBSA methods. Due to its high binding affinity with the receptor molecule, ligand MMs02998601 with the binding affinity of −10.1 kcal/mol was selected as the best docking hit, while on the basis of free energy calculations, MMs02321984 was rescored as a top hit followed by MMs02998601. Briefly, MMs02321984 and MMs02998601 are the top most priorities for the recently resolved structure of ZIKV NS5 RNA dependent RNA polymerase, which need to be evaluated in *in vitro* and *in vivo* studies to confirm their high inhibitory activity.

Declaration of Competing Interest

The authors declare that they have no known competing financial interests or personal relationships that could have appeared to influence the work reported in this paper.

Acknowledgements

Appendix A. Supplementary material

Supplementary data to this article can be found online at https://doi.org/10.1016/j.jsps.2020.10.005.

References

Abbasi, S., Raza, S., Azam, S.S., Liedl, K.R., Fuchs, J.E., 2016. Interaction mechanisms of a melatonergic inhibitor in the melatonin synthesis pathway. J. Mol. Liq. 221, 507–517.

Abro, A., Azam, S.S., 2016. Binding free energy based analysis of arsenic (+ 3 oxidation state) methyltransferase with S-adenosylmethionine. J. Mol. Liq. 220, 375–382.

Ahmad, N., Badshah, S.L., Junaid, M., Ur Rehman, A., Muhammad, A., Khan, K., 2020a. Structural insights into the Zika virus NS1 protein inhibition using a computational approach. J. Biomol. Struct. Dyn., 1–8

Ahmad, N., Farman, A., Badshah, S.L., Rahman, A.U., ur Rashid, H., Khan, K., 2017. Molecular modeling, simulation and docking study of ebola virus glycoprotein. J. Mol. Graph. Model. 72, 266–271.

Ahmad, N., Rehman, A.U., Badshah, S.L., Ullah, A., Mohammad, A., Khan, K., 2020b. Molecular dynamics simulation of zika virus NS5 RNA dependent RNA polymerase with selected novel non-nucleoside inhibitors. J. Mol. Struct. 1203.

Badshah, S.L., Mabkhot, Y.N., Ahmad, N., Syed, S., Naeem, A., 2018. Zika virus, microcephaly and its possible global spread. Current topics in Zika 13.

Badshah, S.L., Naeem, A., Mabkhot, Y., 2017. The new high resolution crystal structure of NS2B-NS3 protease of Zika virus. Viruses 9, 7.

Best, S.M., 2017. The many faces of the flavivirus NS5 protein in antagonism of type I interferon signaling. J. Virol. 91, e01970–e02016.

Bio-Qiagen, C.L.C., 2016. CLC sequence viewer.

Boldescu, V., Behnam, M.A., Vasilakis, N., Klein, C.D., 2017. Broad-spectrum agents for flaviviral infections: dengue, Zika and beyond. Nat. Rev. Drug Discovery 16, 565.

Brylinski, M., Skolnick, J., 2008. A threading-based method (FINDSITE) for ligand-binding site prediction and functional annotation. Proc. Natl. Acad. Sci. 105, 129–134.

Burley, S.K., Berman, H.M., Kleywegt, G.J., Markley, J.L., Nakamura, H., Velankar, S., 2017. Protein Data Bank (PDB): the single global macromolecular structure archive Protein Crystallography. Springer, 627–641.

Butcher, S.J., Grimes, J.M., Makeyev, E.V., Bamford, D.H., Stuart, D.I., 2001. A mechanism for initiating RNA-dependent RNA polymerization. Nature 410, 235–240.

Capra, J.A., Laskowski, R.A., Thornton, J.M., Singh, M., Funkhouser, T.A., 2009. Predicting protein ligand binding sites by combining evolutionary sequence conservation and 3D structure. PLoS computational biology 5.

Chan, J.F., Choi, G.K., Yip, C.C., Cheng, V.C., Yuen, K.-Y., 2016. Zika fever and congenital Zika syndrome: an unexpected emerging arboviral disease. J. Infect. 72, 507–524.

Chaudhary, V., Yuen, K.-S., Chan, J.F.-W., Chan, Ching-Ping, Wang, P.-H., Cai, J.-P., Zhang, S., Liang, M., Kok, K.-H., Chan, Chi-Ping, 2017. Selective activation of type II interferon signaling by Zika virus NS5 protein. J. Virol. 91, e00163–e00217.

Chen, D., Oezguen, N., Urvil, P., Ferguson, C., Dann, S.M., Savidge, T.C., 2016. Regulation of protein-ligand binding affinity by hydrogen bond pairing. Sci. Adv. 2.

Chen, L.H., Hamer, D.H., 2016. Zika virus: rapid spread in the western hemisphere. Ann. Intern. Med. 164, 613–615.

Choi, K.H., Rossmann, M.G., 2009. RNA-dependent RNA polymerases from Flaviviridae. Curr. Opin. Struct. Biol. 19, 746–751.

Daina, A., Michielin, O., Zoete, V., 2017. SwissADME: a free web tool to evaluate pharmacokinetics, drug-likeness and medicinal chemistry friendliness of small molecules. Sci. Rep. 7, 42717.

Dallakyan, S., Olson, A.J., 2015. Chapter 19 Small-Molecule Library Screening by Docking with PyRx 1263, 243–250. https://doi.org/10.1007/978-1-4939-2269-7

Duan, W., Song, H., Wang, H., Chai, Y., Su, C., Qi, J., Shi, Y., Gao, G.F., 2017. The crystal structure of Zika virus NS5 reveals conserved drug targets. The EMBO J. 36, 919–933.

Feranchuk, S., Potapova, U., Belikov, S., 2016. Virtual screening of inhibitors for the Zika virus proteins. bioRxiv 060798.

Floris, M., Masciocchi, J., Fanton, M., Moro, S., 2011. Swimming into peptidomimetic chemical space using pepMMsMIMIC 39, 261–269. https://doi.org/10.1093/nar/gkr287

Godoy, A.S., Lima, G.M., Oliveira, K.I., Torres, N.U., Maluf, F.V., Guido, R.V., Oliva, G., 2017. Crystal structure of Zika virus NS5 RNA-dependent RNA polymerase. Nat. Commun. 8, 1–6.

Goodsell, D.S., Zardecki, C., Di Costanzo, L., Duarte, J.M., Hudson, B.P., Persikova, I., Segura, J., Shao, C., Voigt, M., Westbrook, J.D., 2020. RCSB Protein Data Bank: Enabling biomedical research and drug discovery. Protein Sci. 29, 52–65.

Gore, S., García, E.S., Hendrickx, P.M., Gutmanas, A., Westbrook, J.D., Yang, H., Feng, Z., Baskaran, K., Berrisford, J.M., Hudson, B.P., 2017. Validation of structures in the protein data bank. Structure 25, 1916–1927.

Hilgenfeld, R., 2016. Zika virus NS1, a pathogenicity factor with many faces. The EMBO J. 35, 2631–2633.

Irwin, J.J., Shoichet, B.K., 2005. ZINC - A free database of commercially available compounds for virtual screening 177–182.

Kazmi, S.S., Ali, W., Bibi, N., Nouroz, F., 2020. A review on Zika virus outbreak, epidemiology, transmission and infection dynamics. J. Biol. Res. Thessaloniki 27, 1–11.

Keating, G.M., Vaidya, A., 2014. Sofosbuvir: first global approval. Drugs 74, 273–282.

Kishimoto, T.K., Viswanathan, K., Ganguly, T., Elankumaran, S., Smith, S., Pelzer, K., Lansing, J.C., Sriranganathan, N., Zhao, G., Galcheva-Gargova, Z., Al-Hakim, A., Bailey, G.S., Fraser, B., Roy, S., Rogers-Cotrone, T., Buhse, L., Whary, M., Fox, J., Nasr, M., Dal Pan, G.J., Shriver, Z., Langer, R.S., Venkataraman, G., Austen, K.F., Woodcock, J., Sasisekharan, R., 2008. Contaminated heparin associated with adverse clinical events and activation of the contact system. N. Engl. J. Med. https://doi.org/10.1056/nejmoa0803200.

Lionta, E., Spyrou, G., Vassilatis, K.D., Cournia, Z., 2014. Structure-based virtual screening for drug discovery: principles, applications and recent advances. Curr. Top. Med. Chem. 14, 1923–1938.

Malet, H., Massé, N., Selisko, B., Romette, J.-L., Alvarez, K., Guillemot, J.C., Tolou, H., Yap, T.L., Vasudevan, S.G., Lescar, J., 2008. The flavivirus polymerase as a target for drug discovery. Antiviral Res. 80, 23–35.

Miller III, B.R., McGee Jr, T.D., Swails, J.M., Homeyer, N., Gohlke, H., Roitberg, A.E., 2012. MMPBSA. py: an efficient program for end-state free energy calculations. J. Chem. Theory Comput. 8, 3314–3321.

Musso, D., Ko, A.I., Baud, D., 2019. Zika virus infection—after the pandemic. N. Engl. J. Med. 381, 1444–1457. https://doi.org/10.1056/NEJMra1808246.

Ng, K.K.-S., Arnold, J.J., Cameron, C.E., 2008. Structure-function relationships among RNA-dependent RNA polymerases. RNA Interference. Springer, 137–156.

Olsen, D.B., Eldrup, A.B., Bartholomew, L., Bhat, B., Bosserman, M.R., Ceccacci, A., Colwell, L.F., Fay, J.F., Flores, O.A., Getty, K.L., 2004. A 7-deaza-adenosine analog is a potent and selective inhibitor of hepatitis C virus replication with excellent pharmacokinetic properties. Antimicrob. Agents Chemother. 48, 3944–3953.

Ou-Yang, S., Lu, J., Kong, X., Liang, Z., Luo, C., Jiang, H., 2012. Computational drug discovery. Acta Pharmacol. Sin. 33, 1131–1140.

Parkinson, T., Pryde, D.C., 2010. Small molecule drug discovery for Dengue and West Nile viruses: applying experience from hepatitis C virus. Future Med. Chem. 2, 1181–1203.

Pattnaik, A., Palermo, N., Sahoo, B.R., Yuan, Z., Hu, D., Annamalai, A.S., Vu, H.L., Correas, I., Prathipati, P.K., Destache, C.J., 2018. Discovery of a non-nucleoside RNA polymerase inhibitor for blocking Zika virus replication through in silico screening. Antiviral Res. 151, 78–86.

Ramharack, P., Soliman, M.E., 2018. Zika virus NS5 protein potential inhibitors: an enhanced in silico approach in drug discovery. J. Biomol. Struct. Dyn. 36, 1118–1133.

Rey, J., Lagorce, D., Vavru, M., Labb, M., Miteva, M.A., Sperandio, O., Villoutreix, B.O., Tuff, P., 2015. MTiOpenScreen : a web server for structure-based 43, 448–454. https://doi.org/10.1093/nar/gkv306

Saiz, J.-C., Vázquez-Calvo, Á., Blázquez, A.B., Merino-Ramos, T., Escribano-Romero, E., Martín-Acebes, M.A., 2016. Zika virus: the latest newcomer. Front. Microbiol. 7, 496.

Song, L.F., Lee, T.-S., Zhu, C., York, D.M., Merz Jr, K.M., 2019. Using AMBER18 for relative free energy calculations. J. Chem. Inf. Model. 59, 3128–3135.

Studio, D., 2009. version 2.5. Accelrys Inc.: San Diego, CA, USA.

Upadhyay, A.K., Cyr, M., Longenecker, K., Tripathi, R., Sun, C., Kempf, D.J., 2017. Crystal structure of full-length Zika virus NS5 protein reveals a conformation similar to Japanese encephalitis virus NS5. Acta Crystallographica Section F: Struct. Biol. Commun. 73, 116–122.

Wang, B., Tan, X.-F., Thurmond, S., Zhang, Z.-M., Lin, A., Hai, R., Song, J., 2017. The structure of Zika virus NS5 reveals a conserved domain conformation. Nat. Commun. 8, 1–6.

Wang, B., Thurmond, S., Hai, R., Song, J., 2018. Structure and function of Zika virus NS5 protein : perspectives for drug design. Cell. Mol. Life Sci. https://doi.org/10.1007/s00018-018-2751-x.

Wass, M.N., Kelley, L.A., Sternberg, M.J., 2010. 3DLigandSite: predicting ligand-binding sites using similar structures. Nucleic Acids Res. 38, W469–W473.

Yang, J., Roy, A., Zhang, Y., 2013. Protein–ligand binding site recognition using complementary binding-specific substructure comparison and sequence profile alignment. Bioinformatics 29, 2588–2595.

Yap, T.L., Xu, T., Chen, Y.-L., Malet, H., Egloff, M.-P., Canard, B., Vasudevan, S.G., Lescar, J., 2007. Crystal structure of the dengue virus RNA-dependent RNA polymerase catalytic domain at 1.85-angstrom resolution. J. Virol. 81, 4753–4765.

Zhang, C., Freddolino, P.L., Zhang, Y., 2017. COFACTOR: improved protein function prediction by combining structure, sequence and protein–protein interaction information. Nucleic Acids Res. 45, W291–W299.

Zhang, S., 2011. Computer-aided drug discovery and development, in: Drug Design and Discovery. Springer, 23–38.

Zhao, B., Yi, G., Du, F., Chuang, Y.-C., Vaughan, R.C., Sankaran, B., Kao, C.C., Li, P., 2017. Structure and function of the Zika virus full-length NS5 protein. Nat. Commun. 8, 1–9.

Zhao, B., Yi, G., Du, F., Chuang, Y.-C., Vaughan, R.C., Sankaran, B., Kao, C.C., Li, P., 2017. Structure and function of the Zika virus full-length NS5 protein. Nat. Commun. 8, 1–9.